

Optical properties of carbon grains: Influence on dynamical models of AGB stars

Anja C. Andersen¹, Rita Loidl², and Susanne Höfner^{2,3}

¹ Niels Bohr Institute, Astronomical Observatory, Juliane Maries Vej 30, DK-2100 Copenhagen, Denmark (anja@astro.ku.dk)

² Institute for Astronomy, University of Vienna, Türkenschanzstraße 17, A-1180 Vienna, Austria (loidl@astro.univie.ac.at)

³ Uppsala Astronomical Observatory, Box 515, S-75120 Uppsala, Sweden (hoefner@astro.uu.se)

Received 14 April 1999 / Accepted 7 July 1999

Abstract. For amorphous carbon several laboratory extinction data are available, which show quite a wide range of differences due to the structural complexity of this material. We have calculated self-consistent dynamic models of circumstellar dust-shells around carbon-rich asymptotic giant branch stars, based on a number of these data sets. The structure and the wind properties of the dynamical models are directly influenced by the different types of amorphous carbon. In our test models the mass loss is not severely dependent on the difference in the optical properties of the dust, but the influence on the degree of condensation and the final outflow velocity is considerable. Furthermore, the spectral energy distributions and colours resulting from the different data show a much wider spread than the variations within the models due to the variability of the star. Silicon carbide was also considered in the radiative transfer calculations to test its influence on the spectral energy distribution.

Key words: hydrodynamics – radiative transfer – stars: atmospheres – stars: carbon – stars: AGB and post-AGB

1. Introduction

Asymptotic giant branch (AGB) stars show large amplitude pulsations with periods of about 100 to 1000 days. The pulsation creates strong shock waves in the stellar atmosphere, causing a levitation of the outer layers. This cool and relatively dense environment provides favourable conditions for the formation of molecules and dust grains. Dust grains play an important role for the heavy mass loss, which influences the further evolution of the star.

Condensation and evaporation of dust in envelopes of pulsating stars must be treated as a time-dependent process since the time scales for condensation and evaporation are comparable to variations of the thermodynamic conditions in the stellar envelope. The radiation pressure on newly formed dust grains can enhance or even create shock waves leading to more or less pronounced discrete dust shells in the expanding circumstellar flow (e.g. Fleischer et al. 1991, 1992; Höfner et al. 1995; Höfner

& Dorfi 1997). Since a significant part of the dust grains transferred to interstellar space are produced in the atmosphere of these old luminous stars (Sedlmayr 1994) an understanding of the nature of mass loss of these long-period variables is crucial for the general understanding of dust in space.

Modelling circumstellar envelopes requires knowledge of the absorption properties of the different types of grains over the relevant part of the electromagnetic spectrum. For this the optical properties of the corresponding dust material are needed. Amorphous carbon is a very good candidate as the most common type of carbon grains present in circumstellar envelopes, since the far-infrared data of late-type stars show a spectral index as expected for a very disordered two-dimensional material like amorphous carbon (Huffman 1988).

Silicon carbide (SiC) grains seem to be another important component of the dust in circumstellar envelopes. While amorphous carbon could explain the continuum emission, SiC particles could be responsible for the 11.3 μm band observed in many C-rich objects.

In this paper, we present self-consistent dynamical models of circumstellar dust shells calculated with selected laboratory amorphous carbon data. Based on these models we have performed radiative transfer calculations for pure amorphous carbon and in some cases also including SiC dust. In Sect. 3 the used amorphous carbon data are described. The influence on the model structure is described in Sect. 4 and the resulting spectral appearance is discussed in Sect. 5.

2. Optical properties of dust

The two sets of quantities that are used to describe optical properties of solids are the real and imaginary parts of the complex refractive index $m = n + ik$ and the real and imaginary parts of the complex dielectric function (or relative permittivity) $\epsilon = \epsilon' + i\epsilon''$. These two sets of quantities are not independent, the complex dielectric function ϵ is related to the complex refractive index, m , by $\epsilon' = n^2 - k^2$ and $\epsilon'' = 2nk$, when the material is assumed to be non-magnetic ($\mu = \mu_0$). Reflection and transmission by bulk media are best described using the complex refractive index, m , whereas absorption and scattering by par-

ticles which are small compared with the wavelength are best described by the complex dielectric function, ϵ .

The problem of evaluating the expected spectral dependence of extinction for a given grain model (i.e. assumed composition and size distribution) is essentially that of evaluating the extinction efficiency Q_{ext} . It is the sum of corresponding quantities for absorption and scattering; $Q_{\text{ext}} = Q_{\text{abs}} + Q_{\text{sca}}$. These efficiencies are functions of two quantities; a dimension-less size parameter $x = 2\pi a/\lambda$ (where a = the grain radius and λ = the wavelength) and a composition parameter, the complex refractive index m of the grain material. Q_{abs} and Q_{sca} can therefore be calculated from the complex refractive index using Mie theory for any assumed grain model. The resulting values of total extinction can be compared with observational data.

A limit case within the Mie theory is the Rayleigh approximation for spherical particles. This approximation is valid when the grains are small compared to the wavelength, $x = 2\pi a/\lambda \ll 1$ and in the limit of zero phase shift in the particle ($|m|x \ll 1$). In the Rayleigh approximation the extinction by a sphere in vacuum is given as:

$$\frac{Q_{\text{ext}}}{a} = \frac{8\pi}{\lambda} \text{Im} \left\{ \frac{m^2 - 1}{m^2 + 2} \right\}. \quad (1)$$

2.1. Measuring methods of optical properties

A proper application of Mie theory to experimental data requires that the samples are prepared such that the particles are quite small (usually sub-micrometer), well isolated from one another, and that the total mass of particles is accurately known.

In order to obtain single isolated homogeneous particles, the grains are often dispersed in a solid matrix. Small quantities of sample are mixed thoroughly with the powdered matrix material e.g. KBr or CsI. The matrix is pressed into a pellet which has a bulk transparency in the desired wavelength region. Some of the problems with this technique are that there is a tendency for the sample to clump along the outside rim of the large matrix grains and that the introduction of a matrix, which has a refractive index different from vacuum, might influence the band shape and profile. This matrix effect can be a problem for comparisons of laboratory measurements with astronomical spectra (Papoular et al. 1998; Mutschke et al. 1999).

By measuring the sample on a substrate (e.g. quartz, KBr, Si or NaCl) using e.g. an infrared microscope, the matrix effect can nearly be avoided since the sample is almost fully surrounded by a gas (e.g. air, Ar or He). But the amount of material in the microscopic aperture remains unknown, which is an important disadvantage of this method. Therefore, these measurements are not quantitative but they reveal the shape of the spectrum nearly without a matrix effect (Mutschke et al. 1999).

A major problem of both methods is clustering of the grain samples either during the production of the particles or within the matrix or on the substrate. Clustering can cause a dramatic difference in the optical properties (Huffman 1988). A way to avoid this problem is to perform the optical measurements on a polished bulk sample. For the determination of both n and k two

or more measurements on bulk samples are required. This might be done either by a transmission and a reflection measurement, or by two reflectance measurements determinations at different angles or with different polarisations. Since the real part, n , of the refractive index, m , is determined by the phase velocity and the imaginary part, k , by the absorption, a transmission measurement easily fixes k . The Kramers-Kronig relations can be applied in order to obtain the optical constants for grain measurements. The real part of the refractive index can be expressed as an integral of the imaginary part (see e.g. Bohren & Huffman 1983).

3. Carbon grains

While carbon is expected to constitute a major fraction of the circumstellar dust in carbon stars, its exact form is still unclear. Carbon has the unique property that the atoms can form three different types of bonds through sp^1 , sp^2 (graphite) and sp^3 (diamond) hybridization.

A number of observations of late-type stars contradict the presence of graphite as the dominant dust type (e.g. Campbell et al. 1976; Sopka et al. 1985; Martin & Rogers 1987; Gürtler et al. 1996). The far-infrared (FIR) data of late-type stars generally show a dust emissivity law of $Q(\lambda) \sim \lambda^{-\beta}$ with a spectral index of $\beta \approx 1$. While graphite grains have a FIR emission proportional to λ^{-2} (Draine & Lee 1984), a λ^{-1} behaviour can be expected in a very disordered two-dimensional material like amorphous material (Huffman 1988; Jäger et al. 1998).

Amorphous carbon grains therefore seem to be a very good candidate as the common type of carbon grains present in circumstellar envelopes. Another possibility could be small diamond grains. Presolar diamond grains have been identified from primitive (unaltered) meteorites (carbonaceous chondrites) and are the most abundant (500 ppm) of the presolar grains discovered so far (Lewis et al. 1987). At least 3% of the total amount of carbon present at the formation of the Solar System was in the form of diamonds (Huss & Lewis 1994). The place of origin of the presolar diamonds is still unknown, but since they can only have formed under reducing conditions Jørgensen (1988) has suggested C-rich AGB stars as the place of formation of the majority of the presolar diamond grains.

It has been suggested by Krüger et al. (1996) that the surface growth processes on carbonaceous seed particles in circumstellar envelopes will take place at sp^3 bonded carbon atoms rather than at sp^2 bonded ones, which suggests that the grain material formed in circumstellar envelopes could be amorphous-diamond like carbon. Presolar diamonds extracted from meteorites have a median grain size of about 2 nm (Fraundorf et al. 1989), meaning that each diamond contains a few hundred to a few thousand carbon atoms. The presolar diamonds therefore seem to actually consist of a mixture of diamond (core) and hydrogenate amorphous carbon (surface) having about 0.46 the volume fraction of pure diamond (Bernatowicz et al. 1990).

Several spectra of presolar diamonds from various meteorites have been published (Lewis et al. 1989; Colangeli et al. 1995; Mutschke et al. 1995; Hill et al. 1997; Andersen et al.

1998; Braatz et al., submitted to Meteorit. Planet. Sci.) and even though a number of artifacts tends to be present in all the spectra, the general trend is that the presolar diamonds have an absorption coefficient that is twice that of pure diamond and a factor of a hundred less than the “diamond-like” amorphous carbon of Jäger et al. (1998).

There exists a wide variety of possible amorphous carbon grain types, which fall in between the categories “diamond-like” and “graphite-like” amorphous carbon. We have calculated dynamical models using various laboratory data of amorphous carbon to determine the possible influence of these different grain types on the structure and the wind properties of C-rich AGB star models.

3.1. Laboratory measurements of amorphous carbon

Laboratory conditions are far from the actual space conditions where grains are produced or processed, but experiments in which physical and chemical parameters are controlled and monitored do give the option of selecting materials which may match the astronomical observations. When choosing which amorphous carbon data to use one is faced with the fact that due to the various processes used in the sample preparation, differences often appear between the measurements of various authors. Another major problem is that the optical properties of amorphous carbon are most often obtained by different techniques in different wavelength regions. Extinction measurements of sub-micron-sized particles is the most common technique in the infrared. In the visible and ultraviolet, reflectivity and transmission measurements are often obtained on bulk samples.

Bussoletti et al. (1987a) have determined the extinction efficiencies for various types of sub-micron amorphous carbon particles and spectroscopically analysed them in the wavelength range $1000 \text{ \AA} - 300 \mu\text{m}$. In their paper they present an updated version of the data already published from 2000 \AA to $40 \mu\text{m}$ (Borghesi et al. 1983, 1985a) and new data obtained in the UV/vis ($1000-3000 \text{ \AA}$) and in the FIR ($35-300 \mu\text{m}$). The sub-micron amorphous carbon grains were obtained by means of two methods: (1) striking an arc between two amorphous carbon electrodes in a controlled Ar atmosphere at different pressures (samples AC1, AC2 and AC3; where the numbers refer to different accumulation distances from the arc discharge); (2) burning hydrocarbons (benzene and xylene) in air at room pressure (samples BE and XY). The smoke was collected on quartz substrates. For the UV/vis spectroscopy the quartz substrates on which the particles had been collected were used directly while the dust was scrapped from the substrate and embedded in KBr pellets for the IR spectroscopy. Bussoletti et al. (1987b) suggest that the extinction efficiencies, Q_{ext}/a , for the AC samples should be corrected by a factor of 5 due to an experimental underestimation of the pellet density. This correction gives an agreement with the data by Koike et al. (1980).

Colangeli et al. (1995) measured the extinction efficiency in the range $40 \text{ nm} - 2 \text{ mm}$. They produced three different samples; two by arc discharge between amorphous carbon electrodes in

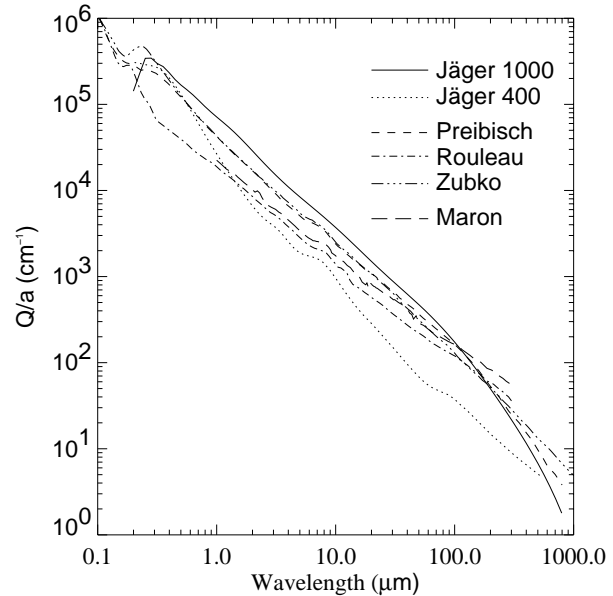


Fig. 1. Calculated extinction efficiency of amorphous carbon from optical constants published by Maron (1990), Rouleau & Martin (1991), Preibisch et al. (1993), Zubko et al. (1996) and Jäger et al. (1998), see Table 1 for annotations. The extinction efficiency factors were calculated from the optical constants (n and k) in the Rayleigh approximation for spheres.

Ar and H_2 atmospheres at 10 mbar (sample ACAR and ACH2 respectively) and one by burning benzene in air (sample BE). The samples were deposited onto different substrates for the UV/vis measurements, while in the IR the samples were prepared both on a substrate and by being embedded in KBr/CsI pellets and for the FIR measurements the samples were embedded in polyethylene pellets. These different but overlapping methods gave the possibility of evaluating the difference as a result of embedding the samples in a matrix or by having them on a substrate. Colangeli et al. (1995) found that embedding the samples in a matrix introduces a systematic error (the matrix effect) while the spectra obtained for grains deposited onto a substrate did not suffer from any matrix effect detectable within the accuracy available in the experiment. Therefore the FIR data were corrected for the extinction offset introduced by the matrix.

Jäger et al. (1998) produced structurally different carbon materials by pyrolyzing cellulose materials at different temperatures (400°C , 600°C , 800°C and 1000°C), and characterised them in great detail. These materials have increasing sp^2/sp^3 ratios making the amorphous carbon pyrolysed at 400°C the most “diamond-like” with the lowest sp^2/sp^3 ratio while the amorphous carbon pyrolysed at 1000°C is more “graphite-like” with the highest sp^2/sp^3 ratio. The pyrolysed carbon samples were embedded in epoxy resin and reflectance of the samples was measured in the range $200 \text{ nm} - 500 \mu\text{m}$, making this the first consistent laboratory measurement of amorphous carbon over the whole spectral range relevant for radiative transfer calculations of C-rich AGB stars. From the reflectance spectra the complex refractive index, m , was derived by the Lorentz oscillator method (see e.g. Bohren & Huffman 1983, Chap. 9).

There is a significant difference between the two low temperature (400° C and 600° C) and the two high temperature samples (800° C and 1000° C). The latter two behave very similar to glassy carbon.

In contrast to grain measurements, the bulk samples by Jäger et al. (1998) give the possibility of investigating the difference between the influence of the internal structure of amorphous material and the morphology of the carbon grains. These two properties can be separated out due to the careful investigation of the internal structures of the four samples and the range of material properties that these four amorphous carbon samples span (from “diamond-like” to “graphite-like”).

3.2. Calculated optical properties of amorphous carbon

Several authors have used the data of Bussoletti et al. (1987a) and Colangeli et al. (1995) to obtain the optical constants of amorphous carbon grains.

Maron (1990) used the extinction efficiencies of Bussoletti et al. (1987a) (sample AC2) to derive the optical constants (n and k) by estimating the complex permittivity by a combination of the measured absorption efficiencies, dispersion formulae and Kramers-Kronig relation. The reason for performing these calculations is that the optical constants are needed for modelling emission properties of grains containing various allotropic carbons or having different sizes. Maron (1990) is of the opinion that the differences between the primary extinction efficiencies obtained by Bussoletti et al. (1987a) and Koike et al. (1980) are real and caused rather by the use of different electrodes (amorphous carbon and graphite, respectively) than by an underestimation of the pellet column density as suggested by Bussoletti et al. (1987b). Therefore he did not introduce the correction suggested by Bussoletti et al. (1987b).

Rouleau & Martin (1991) used the AC2 and BE data from Bussoletti et al. (1987a) to produce synthetic optical constants (n and k) which satisfy the Kramers-Kronig relations and highlight the effects of assuming various shape distributions and fractal clusters. One of the complications in determining these optical properties of amorphous carbon material was that in the infrared the extinction measurements were done on a sample of sub-micron-sized particles, while in the visible and ultraviolet the optical constants were obtained by measurements of reflectivity and transmission or by electron energy loss spectroscopy on bulk samples. These diverse measurements were used to produce synthetic optical constants which satisfied the Kramers-Kronig relations.

Preibisch et al. (1993) used the BE sample from Bussoletti et al. (1987a) between 0.1–300 μm and the data of Blanco et al. (1991) between 40–700 μm , using the same technique as used by Rouleau & Martin (1991) for deriving optical constants taking shape and clustering effects into account. Preibisch et al. (1993) extend the available optical constants on the basis of the measurements of Blanco et al. (1991). With these they determine the opacities of core-mantle-particles with varying mantle thickness and pollution.

Zubko et al. (1996) used the extinction efficiencies obtained by Colangeli et al. (1995) to derive the optical constants (n and k) also by use of the Kramers-Kronig approach. These data were used to evaluate the possible shapes of the amorphous carbon grains in space and the possible clustering of the particles.

In this study we have used the derived optical constants of Maron (1990), Rouleau & Martin (1991), Preibisch et al. (1993), Zubko et al. (1996) and Jäger et al. (1998), see Table 1 for details. The extinction efficiency data presented in this paper were calculated in the Rayleigh approximation for spheres.

3.3. The nature of silicon carbide

Thermodynamic equilibrium calculations performed by Friedemann (1969a,b) and Gilman (1969) suggested that SiC particles can form in the mass outflow of C-rich AGB stars. The observations performed by Hackwell (1972) and Treffers & Cohen (1974) presented the first empirical evidence for the presence of SiC particles in stellar atmospheres. A broad infrared emission feature seen in the spectra of many carbon stars, peaking between 11.0 and 11.5 μm is therefore attributed to solid SiC particles and SiC is believed to be a significant constituent of the dust around carbon stars.

An ultimate proof for the formation of SiC grains in C-rich stellar atmospheres was the detection of isotropically anomalous SiC grains in primitive meteorites (Bernatowicz et al. 1987). Based on isotopic measurements of the major and trace elements in the SiC grains and on models of stellar nucleosynthesis, it is established that a majority of the presolar SiC grains has their origin in the atmospheres of late-type C-rich stars (Gallino et al. 1990, 1994; Hoppe et al. 1994). For recent reviews see, e.g., Anders & Zinner (1993), Ott (1993) and Hoppe & Ott (1997).

Detailed laboratory investigations on the infrared spectrum of SiC have been presented by the following authors: Spitzer et al. (1959a,b) performed thin film measurements on β - and α -SiC; Stephens (1980) measured on crystalline β -SiC smokes; Friedemann et al. (1981) measured two commercially available α -SiC; Borghesi et al. (1985b) investigated three commercially produced α - and one commercially produced β -SiC; Papoular et al. (1998) measured two samples of β -SiC powders, one produced by laser pyrolysis and one which was commercially available; Mutschke et al. (1999) studied 16 different SiC powders which were partly of commercial origin and partly laboratory products (8 α -SiC and 8 β -SiC); Speck et al. (1999) made thin film measurements of α - and β -SiC and Andersen et al. (1999) have measured the spectrum of meteoritic SiC.

One of the difficulties in interpreting laboratory data lies in disentangling the combination of several effects due to size, shape, physical state (amorphous or crystalline), purity of the sample and possible matrix effects if a matrix is used. There is a general agreement that grain size and grain shape have a crucial influence on the absorption feature of SiC particles. This is particularly demonstrated by Papoular et al. (1998), Andersen et al. (1999) and Mutschke et al. (1999). Papoular et al. (1998), Mutschke et al. (1999) and Speck et al. (1999) have shown that the matrix effect does not shift the resonance feature as a whole

Table 1. Comparison of the different laboratory data and a list of authors who have obtained optical constants from these data.

Reference	Material name	ρ (g/cm ³)	Wavelength interval (μm)	Designation in this paper	Comments
Bussoletti et al. (1987a)	AC2	1.85	0.1–300	Bussoletti AC-2	Arc discharge
Bussoletti et al. (1987a)	BE	1.81 ¹	0.2–300	Bussoletti BE	burning benzene
Bussoletti et al. (1987a)	XY		0.2–300	Bussoletti XY	burning Xylene
Colangeli et al. (1995)	ACAR	1.87	0.04–2000	Colangeli AC	arc discharge in Ar
Colangeli et al. (1995)	ACH2		0.04–950	Colangeli ACH2	arc discharge in H ₂
Colangeli et al. (1995)	BE		0.05–2000	Colangeli BE	burning benzene
Jäger et al. (1998)	cel400	1.435	0.02–500	Jäger 400	most diamond-like
Jäger et al. (1998)	cel600	1.670	0.02–500	Jäger 600	
Jäger et al. (1998)	cel800	1.843	0.02–500	Jäger 800	
Jäger et al. (1998)	cel1000	1.988	0.02–500	Jäger 1000	most graphite-like
Maron (1990)	AC2			Maron	n & k from Bussoletti et al. (1987a)
Rouleau & Martin (1991)	AC2			Rouleau	n & k from Bussoletti et al. (1987a)
Preibisch et al. (1993)	BE			Preibisch	n & k from Bussoletti et al. (1987a)
Zubko et al. (1996)	ACAR			Zubko	n & k from Colangeli et al. (1995)

¹ Given in Rouleau & Martin (1991).

as it was assumed by Friedemann et al. (1981) and Borghesi et al. (1985b). While Papoular et al. (1998) and Mutschke et al. (1999) find that the profile is not shifted but altered, Speck et al. (1999) state that the profile is not affected at all, whether a matrix is used in the experimental set up or not. The influence of purity of the laboratory samples was mainly studied by Mutschke et al. (1999). Another issue considered is the effect of the crystal type. Silicon carbide shows pronounced polytypism which means that there exist a number of possible crystal types differing in only one spatial direction. All these polytypes are variants of the same basic structure and can therefore be divided into two basic groups: α -SiC (the hexagonal polytypes) and β -SiC (the cubic polytype). It was found by Spitzer et al. (1959a,b), Papoular et al. (1998), Andersen et al. (1999) and Mutschke et al. (1999) that the crystal structure of SiC cannot be determined from IR spectra, because there is no systematic dependence of the band profile on the crystal type. In contrast, Borghesi et al. (1985b) and Speck et al. (1999) find the contrary result.

In this paper we have used the average value for bulk SiC reflectance spectra of β -SiC as presented by Mutschke et al. (1999) with $\epsilon_\infty = 6.49$, $\omega_{\text{TO}} = 795.4 \text{ cm}^{-1}$, $\omega_{\text{p}} = 1423.3 \text{ cm}^{-1}$ and $\gamma = 10$ to calculate the optical constants n and k , using the one-oscillator model described in Mutschke et al. (1999). The damping constant γ is an “ad hoc” parameter, which in a perfect crystal reflects the anharmonicity of the potential curve. A damping constant of $\gamma = 10$ characterises crystals which are not structurally perfect but still far from amorphousness.

Since there is no systematic dependence of the band profile on the crystal type in the data of Mutschke et al. (1999), we could just as well have used the data of one of their α -SiC samples and would have obtained a similar result.

The optical constants n and k were used to calculate the extinction efficiency for small spherical grains in the Rayleigh limit. Spheres are not necessarily the best approximation for the grain shape of SiC particles in C-rich AGB stars compared to e.g. a continuous distribution of ellipsoids (CDE) as introduced

by Bohren & Huffman (1983). The general appearance of the feature as well as the peak position will depend on the grain shape, however, common for all grain shapes of SiC are that the feature will always fall between the transverse (TO) and the longitudinal (LO) optical phonon mode, so the difference will be that a spherical grain shape will give rise to a sharper and narrower resonance than other grain shape approximations.

4. Dynamical models

4.1. Modelling method

To obtain the structure of the stellar atmosphere and circumstellar envelope as a function of time we solve the coupled system of radiation hydrodynamics and time-dependent dust formation (cf. Höfner et al. 1995, Höfner & Dorfi 1997 and references therein). The gas dynamics is described by the equations of continuity, motion and energy, and the radiation field by the grey moment equations of the radiative transfer equation (including a variable Eddington factor). In contrast to the models presented in Höfner & Dorfi (1997) we use a Planck mean gas absorption coefficient based on detailed molecular data as described in Höfner et al. (1998). Dust formation is treated by the so-called moment method (Gail & Sedlmayr 1988; Gauger et al. 1990). We consider the formation of amorphous carbon in circumstellar envelopes of C-rich AGB stars.

The dynamical calculations start with an initial model which represents the full hydrostatic limit case of the grey radiation hydrodynamics equations. It is determined by the following parameters: luminosity L_* , mass M_* , effective temperature T_* and the elemental abundances. We assume all elemental abundances to be solar except the one of carbon which is specified by an additional parameter, i.e. the carbon-to-oxygen ratio $\epsilon_{\text{C}}/\epsilon_{\text{O}}$. The stellar pulsation is simulated by a variable boundary (piston) which is located beneath the stellar photosphere and is moving sinusoidally with a velocity amplitude Δu_{p} and a period P .

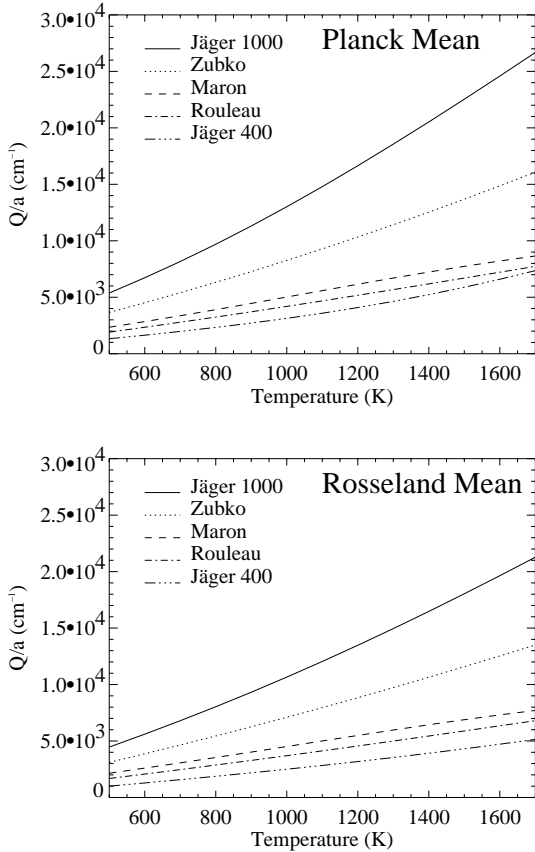


Fig. 2. The Planck mean and the Rosseland mean calculated from the optical constants of amorphous carbon as derived from various experiments. See Table 1 for details. The *Preibisch* data would fall right on top of the *Rouleau* data.

Since the radiative flux is kept constant at the inner boundary throughout the cycle the luminosity there varies according to $L_{\text{in}}(t) \propto R_{\text{in}}(t)^2$.

4.2. Dust opacities

The self-consistent modelling of circumstellar dust shells requires the knowledge of the extinction efficiency Q_{ext} of the grains, or rather of the quantity Q_{ext}/a , which is independent of a in the small particle limit which is applicable in this context. For the models of long period variables presented in Höfner & Dorfi (1997) and Höfner et al. (1998) a fit formula for the Rosseland mean of Q_{ext}/a derived from the optical constants of Maron (1990) was used.

One important point of this paper is to investigate the direct influence of Q_{ext}/a on the structure and wind properties of the dynamical models. Therefore we have computed Rosseland and Planck mean values of Q_{ext}/a (see Fig. 2) based on various optical constants derived from laboratory experiments (see Sect. 3 for details about the samples).

For the dynamical calculations presented here we have selected the following data sets (see Table 1 for a detailed specification): *Jäger400* and *Jäger1000* (representing the extreme

Table 2. Comparison of modelling results for different dust opacity data: mass loss rate \dot{M} (in M_{\odot}/yr), mean velocity at the outer boundary $\langle u \rangle$ (in km s^{-1}), mean degree of condensation at the outer boundary $\langle f_c \rangle$; model parameters: $L_{\star} = 13000 L_{\odot}$, $M_{\star} = 1.0 M_{\odot}$, $T_{\star} = 2700 \text{ K}$, $\varepsilon_{\text{C}}/\varepsilon_{\text{O}} = 1.4$, $P = 650 \text{ d}$, $\Delta u_{\text{p}} = 4 \text{ km s}^{-1}$; ‘R’ denotes a Rosseland mean dust absorption coefficient, ‘P’ a Planck mean; for details see text.

model	data	mean	\dot{M}	$\langle u \rangle$	$\langle f_c \rangle$
DJ1R	<i>Jäger1000</i>	R	$3.1 \cdot 10^{-6}$	14	0.17
DZUR	<i>Zubko</i>	R	$3.3 \cdot 10^{-6}$	13	0.21
DMAR*	<i>Maron</i>	R	$2.9 \cdot 10^{-6}$	11	0.25
DROR	<i>Rouleau</i>	R	$2.7 \cdot 10^{-6}$	11	0.28
DJ4R	<i>Jäger400</i>	R	$2.8 \cdot 10^{-6}$	9	0.35
DJ1P	<i>Jäger1000</i>	P	$3.4 \cdot 10^{-6}$	14	0.15
DJ4P	<i>Jäger400</i>	P	$2.9 \cdot 10^{-6}$	10	0.30

* model P13C14U4 of Höfner et al. (1998)

cases), *Rouleau* (closest to the *Maron* data used in earlier models but extending to wavelengths below $1 \mu\text{m}$) and *Zubko*. The data of *Preibisch* are almost identical to the data of *Rouleau*.

Fig. 2 demonstrates that for a given data set the difference between Planck and Rosseland means is relatively small. This is due to the fact that amorphous carbon grains have a continuous opacity with a smooth wavelength dependence¹.

4.3. Wind properties

All models discussed here are calculated with the same set of stellar parameters, i.e. $L_{\star} = 13000 L_{\odot}$, $M_{\star} = 1.0 M_{\odot}$, $T_{\star} = 2700 \text{ K}$, $\varepsilon_{\text{C}}/\varepsilon_{\text{O}} = 1.4$, $P = 650 \text{ d}$, $\Delta u_{\text{p}} = 4 \text{ km s}^{-1}$, corresponding to model P13C14U4 in Höfner et al. (1998). The only difference between individual models is the adopted mean dust opacity. Most models have been calculated with Rosseland mean dust opacities to allow us a direct comparison with earlier models based on Rosseland means derived from the *Maron* data².

Wind properties like the mass loss rate \dot{M} or the time-averaged outflow velocity $\langle u \rangle$ and degree of condensation $\langle f_c \rangle$ are direct results of the dynamical calculations. The Rosseland mean models in Table 2 (first group) are listed in order of decreasing dust extinction efficiency. Both $\langle u \rangle$ and $\langle f_c \rangle$ change significantly with the dust data used. $\langle f_c \rangle$ increases with decreasing dust extinction efficiency while $\langle u \rangle$ decreases, reflecting a lower optical depth of the circumstellar dust shell (see also Sect. 5). The mass loss rates seem to show a weak overall trend but it is doubtful whether the differences between “neighbouring” models in Table 2 are significant. Since the mass loss rate varies strongly with time the average values given in the table are more uncertain than the ones for the velocity and the degree

¹ In contrast, the two means may differ by orders of magnitude for gas opacities in case of molecular line blanketing.

² Note however that all models use Planck mean gas opacities as discussed in Sect. 4.1.

of condensation which both do not show large variations with time.

The behaviour of the wind properties can be explained in the following way: The stellar parameters of the models presented here were chosen in such a way that the models fall into a domain where dust formation is efficient and the outflow can be easily driven by radiation pressure on dust (luminous, cool star, relatively high C/O ratio). In this case, the mass loss rate is essentially determined by the density in the dust formation zone which mainly depends on stellar and pulsation parameters (see e.g. Höfner & Dorfi 1997). Therefore it is not surprising that the mass loss rates of the different models are quite similar.

On the other hand, in a self-consistent model, the degree of condensation (dust-to-gas ratio) depends both on the thermodynamical conditions in the region where the dust is formed and on the specific grain opacity. The higher the mass absorption coefficient the faster the material is pushed out of the zone where efficient dust formation and grain growth is possible. Therefore the degree of condensation decreases with increasing dust absorption coefficients (i.e. higher radiative pressure) as grain growth is slowed down by dilution of the gas. Note that even in the model with the lowest dust absorption coefficient (DJ4R) the condensation of “free” carbon (i.e. all carbon not locked in CO) is far from complete ($\langle f_c \rangle < 1$).

For the two extreme cases (*Jäger1000* and *Jäger400*) we have also calculated models with Planck mean dust opacities. As shown in Table 2 the wind properties of the corresponding Planck and Rosseland models (DJ1P/DJ1R and DJ4P/DJ4R) are very similar (if the differences are significant at all, see above). The two Planck mean models fit nicely into the dust extinction efficiency sequence discussed before for the Rosseland mean models.

As demonstrated in many earlier papers (e.g. Winters et al. 1994; Höfner & Dorfi 1997) the dust formation in dynamical models is not necessarily periodic with the pulsation period P . In general the models are multi- or non-periodic in the sense that the dust formation cycle is a more or less well defined multiple of P . In the models discussed here, a new dust shell is formed about every 5–6 pulsation periods.

In contrast to the hotter inner regions, the atmospheric structure below about 1500 K does not repeat after each pulsation cycle but is more or less periodic on the dust formation time scales which span several pulsation cycles. While it is easy to compare the time-averaged wind properties of the models it is much more problematic to find comparable “snapshots” in different model sequences for the discussion of observable properties presented in the next section. Therefore in all cases involving detailed radiative transfer on top of given model structures we have decided to show statistical comparisons including several maximum and minimum phase models of each sequence.

5. Spectral energy distributions and synthetic colours

5.1. Frequency-dependent radiative transfer

The dynamical calculation yields the structure of the atmosphere and circumstellar envelope (density, temperature, degree of con-

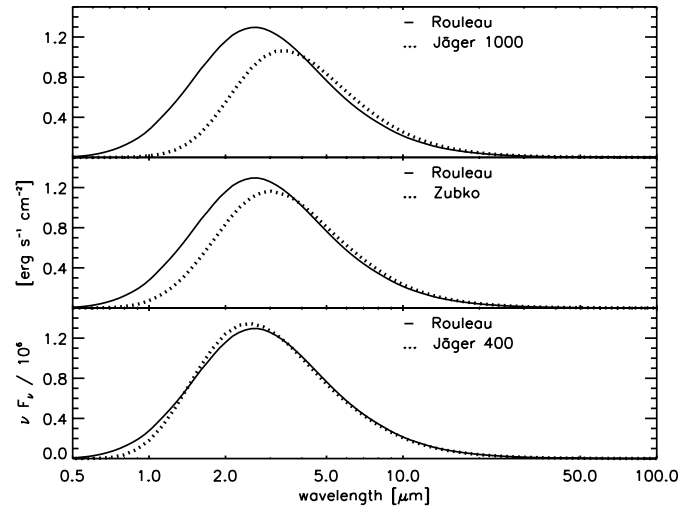


Fig. 3. Spectral energy distributions of a minimum phase model of DROR where the spectra have been calculated with different dust data: we compare *Rouleau* (consistent calculation) with *Jäger1000* (upper), with *Zubko* (middle) and *Jäger400* (lower). For details see text.

denation, etc.) as a function of time. The time-independent radiative transfer equation is solved for each frequency separately along parallel rays to obtain spectral energy distributions (Windsteig et al. 1997 and references therein). The grey gas opacity (Planck mean) is taken directly from the dynamical models. The dust opacity is calculated from the optical properties of amorphous carbon and in some cases SiC (see Sect. 3 for the description of the different dust data).

5.2. Spectral energy distributions

To investigate how the different dust data influence the resulting spectral energy distributions (SEDs), spectra were calculated using the optical constants of amorphous carbon of *Rouleau*, *Zubko*, *Jäger400* and *Jäger1000* on top of a fixed atmospheric structure. Two different kinds of SEDs were calculated; (1) fully consistent ones where the same amorphous carbon data were used in the dynamical model and in the SED calculations and (2) “inconsistent” ones where we used different dust opacity data for the detailed radiative transfer on top of the same dynamical model structure (fixed spatial distribution of density, temperature, degree of condensation). The latter spectra enable us to distinguish between the effect of the various dust data in the radiative transfer calculation and the effect on the model structure.

Fig. 3 shows the result for the SEDs based on a minimum phase model of the DROR model sequence. The full line always denotes the SED of the consistent model where the *Rouleau* data were used for the underlying dynamical model as well as for the calculation of the spectrum. In the upper panel the (inconsistent) *Jäger1000* spectrum (dotted) calculated on top of the same *Rouleau* model is shown in addition to the consistent *Rouleau* spectrum. The middle panel shows the same for *Zubko* and the lower panel for *Jäger400*. The effects of the different

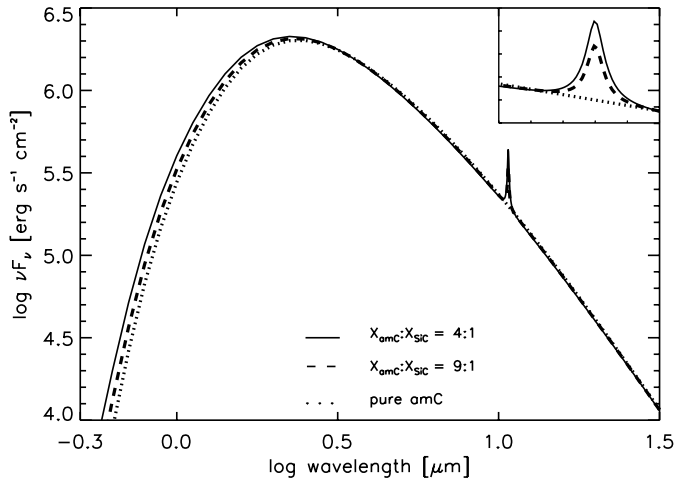


Fig. 4. Spectral energy distributions of a minimum phase model of DJ1R where the spectra have been calculated with amorphous carbon alone (dotted), with a ratio $X_{\text{amC}}:X_{\text{SiC}}$ of 9:1 (dashed) and a ratio of $X_{\text{amC}}:X_{\text{SiC}}$ of 4:1 (solid).

dust data for a given structure compared to a consistent model using the *Rouleau* data can be summarised as follows:

- *Jäger1000*: the spectrum has a lower flux in the short wavelength region (0.5 to 5 μm) and the maximum at longer wavelengths. The lower flux level in this region is due to the fact that Q_{ext}/a for the *Jäger1000* data is higher than for the *Rouleau* data, therefore we have a higher total dust opacity which results in less flux coming out. The shift of the maximum is also due to the higher dust opacity in the *Jäger1000* case.
- *Zubko*: the spectrum has a lower flux level in the short wavelength region and the maximum is shifted to longer wavelengths, but not as far as the *Jäger1000* spectrum. This is due to the fact that *Jäger1000* is a more “graphite-like” amorphous carbon dust than the *Zubko* material.
- *Jäger400*: the spectrum has a comparable flux all over the spectrum and the maximum at slightly shorter wavelengths. The slightly higher flux level around the maximum results from the lower Q_{ext}/a of the *Jäger400* data which is due to its more “diamond-like” nature compared to the *Rouleau* data. In the wavelength region where the maxima of the spectra lie, the two data sets are very similar, therefore the maxima of the SEDs do not differ much in wavelength.

Note that for the “inconsistent” SEDs the total flux may differ from the value of the consistent models.

5.3. Spectral energy distributions including SiC

The analysis of mid-IR carbon star spectra indicates that SiC is the best candidate to reproduce the observations around the 11 μm region. We have therefore considered SiC as an additional dust component (see Sect. 3.3 for details). The formation of SiC is not included in the self-consistent model calculations because (1) little is known about the condensation process and

(2) because we do not expect that SiC will have a significant influence on the model structures. We use either Planck or Roseland means for the model computations and SiC will contribute only in a very narrow wavelength region with small amounts to these mean opacities compared to amorphous carbon.

The effect of SiC as dust component is described in a qualitative manner. The dust opacity κ_{d} for each wavelength is calculated from

$$\kappa_{\text{d}} = \frac{\kappa_{\text{amC}}X_{\text{amC}} + \kappa_{\text{SiC}}X_{\text{SiC}}}{X_{\text{amC}} + X_{\text{SiC}}}$$

where X_i are the fractional parts of amorphous carbon and SiC, respectively, and where κ_{amC} and κ_{SiC} are the opacities of carbon and SiC. Fig. 4 shows how a mixture of dust grains consisting of amorphous carbon (*Jäger1000* data) and SiC modifies the SED around 11.3 μm . Two different ratios of $X_{\text{amC}}:X_{\text{SiC}}$, 4:1 and 9:1 were adopted. The higher the amount of SiC, the stronger is the 11.3 μm feature (see inset of Fig. 4). Another choice of grain shape than spherical for the SiC particles, would result in a broader feature.

5.4. Synthetic colours

For a comparison of the consistent spectra (model structure and spectra computed with the same dust data) we have calculated synthetic J, H and L colours as well as the IRAS 12 μm colour. In a (J–H) versus (H–L) diagram (Fig. 5a) the models based on different amorphous dust data fall into distinct regions.

The models calculated with the *Jäger1000* dust data have the reddest colours in (H–L). The *Jäger400* colours are the bluest, while *Rouleau* and *Zubko* lie in between. In (J–H) models with the *Zubko* data are reddest and the others do not differ much. The reason for the different slopes of *Rouleau* and *Zubko* compared to both of the *Jäger* data sets is that in these cases the maxima of the SEDs are changing between the J and the H filter depending on the phase. The maxima of the SEDs resulting from the *Jäger1000* model structures are always at longer wavelengths and the ones of the *Jäger400* structures lie mainly in one filter. From Fig. 5b, which shows the “inconsistent” colours based on model DROR (structure was calculated with the *Rouleau* data and the spectra with other dust data) in addition to the consistent *Rouleau* colours, it is clear that the influence of the different dust data used in the radiative transfer calculation is much stronger than the effect of the underlying hydrodynamic model structure.

Note that in Fig. 5 only maximum and minimum phases are shown. Other phases would fill in the gaps between successive extremes. The colours are strongly related to the formation of a new dust shell which takes place every 5 to 6 pulsation cycles (see Sect. 4.3). After this time scale the colours match very closely the ones of the preceding dust formation cycle as shown in Fig. 6. When connecting the succeeding points it can be seen that they form a spiral. The minima (circles) are always redder than the following maxima (asterisks).

To investigate also the mid-IR properties of the models we calculated the 12 μm colour. A (L–[12]) vs. (H–L) diagram (Fig. 5c) shows, that again the consistent colours fall into

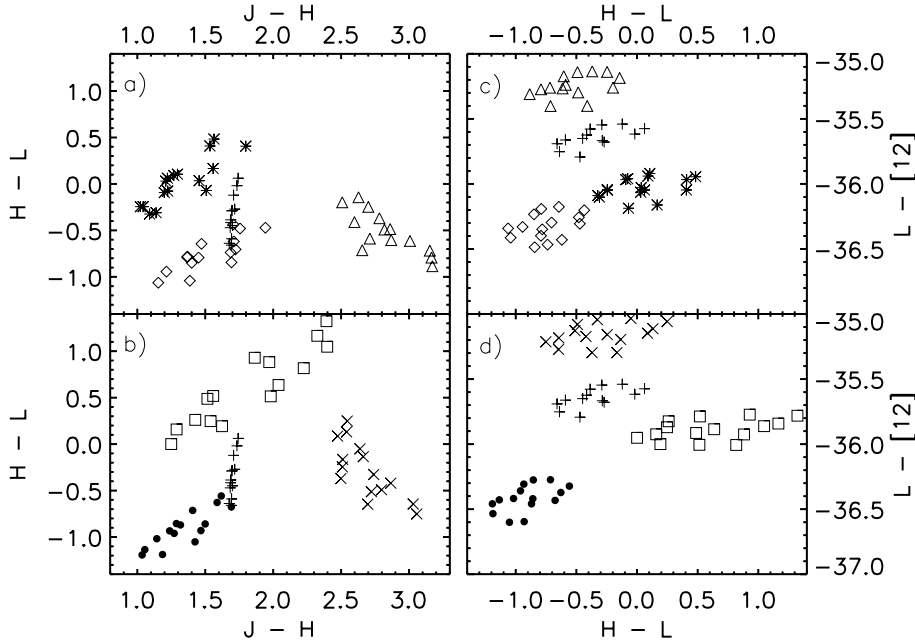


Fig. 5. Synthetic colours: Upper panels: left: $(J-H)$ vs. $(H-L)$ for the maxima and minima of consistent models; crosses denote the *Rouleau* data (DROR), asterisks the *Jäger1000* data (DJ1R), diamonds the *Jäger400* data (DJ4R) and triangles the *Zubko* data (DZUR); right: $(H-L)$ vs. $(L-[12])$ for the same models (same symbols). Lower panels: “inconsistent” colours, all based on model DROR, in comparison to the consistent *Rouleau* colours (crosses): circles represent spectra calculated with the *Jäger400* data, squares denote the *Jäger1000* data and x the *Zubko* dust data. This plot shows that the influence of the different dust data used in the radiative transfer calculation is much stronger than the effect of the model structures.

Table 3. Mean dust optical depths at a few selected wavelengths

optical depth	DJ1R	DZUR	DROR	DJ4R
$\tau_{d,1\mu}$	1.25	1.1	1.0	1.15
$\tau_{d,2.2\mu}$	0.45	0.37	0.37	0.23
$\tau_{d,10\mu}$	0.06	0.08	0.07	0.04

distinct regions. The sequence in $(L-[12])$ (*Zubko - Rouleau - Jäger1000 - Jäger400*) is a sequence of decreasing optical depths. Table 3 lists the mean dust optical depths for a few selected wavelengths. In Fig. 5d the inconsistent colours based on the model structure of DROR are shown for comparison.

From Fig. 5 we can infer that the influence of the different amorphous carbon dust data used in the radiative transfer calculation is much stronger than the effect of the model structures. The colours resulting from the same dust data fall approximately into the same region of a two-colour-diagram, whether they are calculated on top of the corresponding model structure (upper panel) or a fixed model sequence (lower panel). This applies for all data sets.

In addition we computed synthetic colours for the *Maron* and the *Preibisch* data, but they are not shown in Fig. 5 to avoid overlaps in the plot. The *Preibisch* colours fall into the same region as the *Zubko* colours as one would expect because the Q_{ext}/a are very similar. The same applies for the *Maron* and the *Rouleau* data. Only the J flux differs between *Maron* and *Rouleau*, the reason being that the *Maron* data do not extend below $1 \mu\text{m}$ and therefore the corresponding contribution to the J filter is lacking.

6. Summary and conclusions

Carbon bearing grains are expected to form in the outflows of C-rich AGB stars. The two most common types of carbon grains

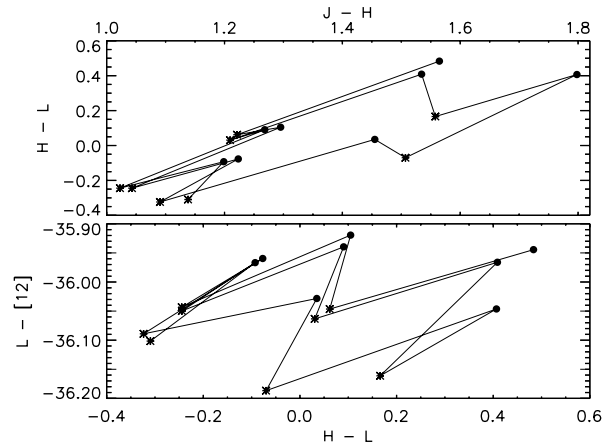


Fig. 6. Upper panel: $(J-H)$ vs. $(H-L)$ for maxima (asterisks) and minima (circles) of the DJ1R model. When connecting the points following each other one can see that the result is a spiral, the minima are always redder than the following maxima. The colours are strongly related to the formation of a new dust shell which takes place every 5 to 6 pulsation cycles. After this time scale the colours match very closely the ones during the formation of the prior dust shell. Lower panel: Same as above, only $(H-L)$ vs. $(L-[12])$ is shown.

in these stars are expected to be amorphous carbon and SiC grains. We have investigated the direct influence of different dust optical properties on the wind characteristics and the resulting observable properties of the dynamical models.

The term amorphous carbon covers a wide variety of material properties from “diamond-like” to “graphite-like”. We have used n and k data of Maron (1990), Rouleau & Martin (1991), Preibisch et al. (1993), Zubko et al. (1996) and Jäger et al. (1998) to investigate the influence of different types of amorphous carbon, on the structure and the wind properties of dynamical models. The Rosseland and Planck mean values of Q_{ext}/a used in

the model computations were calculated from the Rayleigh approximation for spheres. The difference between the Planck and the Rosseland means is relatively small for the amorphous carbon data because the grains have a continuous opacity with a smooth wavelength dependence.

In our test models, both the outflow velocity $\langle u \rangle$ and degree of condensation $\langle f_c \rangle$ change significantly with the dust data used. $\langle f_c \rangle$ increases with decreasing dust extinction efficiency while $\langle u \rangle$ decreases, reflecting a lower optical depth of the circumstellar dust shell. The mass loss rate is, however, not significantly influenced by the use of different dust data.

On top of the structures resulting from the dynamic calculations we have performed detailed radiative transfer calculations to obtain the spectral energy distribution of the circumstellar dust shells. Regarding infrared colours, the influence of the different dust data used in the radiative transfer calculation is much stronger than the effect of the underlying hydrodynamic model structure. However, this should not be used as an excuse for fitting observations by arbitrarily choosing the optical properties of the dust grains for a given model structure. In a consistent model the dynamical properties (e.g. outflow velocities) and the optical appearance of the circumstellar envelope are related in a complex way.

The influence of including SiC grains is that the 11.3 μm feature appears in the spectral energy distribution of the models. How much SiC should be “mixed” into a model to reproduce the 11.3 μm feature observed (e.g. class 4 in Goebel et al. 1995) will very much depend on the assumptions which are made about the size and shape of the SiC grains which enter into the model (Papoular et al. 1998; Andersen et al. 1999; Mutschke et al. 1999).

Acknowledgements. This work was supported by the Austrian Science Fund (FWF, project number S7305-AST) and the Austrian Academy of Sciences (RL acknowledges a “Doktorandenstipendium”). We thank E.A Dorfi (IfA Vienna) for inspiring discussions.

References

- Anders E., Zinner E., 1993, *Meteoritics* 28, 490
- Andersen A.C., Jørgensen U.G., Nicolajsen F., et al., 1998, *A&A* 330, 1080
- Andersen A.C., Jäger C., Mutschke H., et al., 1999, *A&A* 343, 933
- Bernatowicz T., Fraundorf G., Ming T., et al., 1987, *Nat* 330, 728
- Bernatowicz T., Gibbons P.C., Lewis R.S., 1990, *ApJ* 359, 246
- Blanco A., Fonti S., Rizzo F., 1991, *Infrared Phys.* 31, 167
- Bohren C.F., Huffman D.R., 1983, *Absorption and Scattering of Light by Small Particles*. John Wiley & Sons Inc., Toronto
- Borghesi A., Bussoletti E., Colangeli L., et al., 1983, *Infrared Phys.* 23, 85
- Borghesi A., Bussoletti E., Colangeli L., 1985a, *A&A* 142, 225
- Borghesi A., Bussoletti E., Colangeli L., De Blasi C., 1985b, *A&A* 153, 1
- Bussoletti E., Colangeli L., Borghesi A., Orofino V., 1987a, *A&AS* 70, 257
- Bussoletti E., Colangeli L., Orofino V., 1987b, *ApJ* 321, L87
- Campbell M.F., Elias J.H., Gezari D.Y., et al., 1976, *ApJ* 208, 396
- Colangeli L., Menella V., Palumbo P., et al., 1995, *A&AS* 113, 561
- Draine B.T., Lee H.M., 1984, *ApJ* 285, 89
- Fleischer A.J., Gauger A., Sedlmayr E., 1991, *A&A* 242, L1
- Fleischer A.J., Gauger A., Sedlmayr E., 1992, *A&A* 266, 321
- Fraundorf P., Fraundorf G., Bernatowicz T., et al., 1989, *Ultramicroscopy* 27, 401
- Friedemann C., 1969a, *Physica* 41, 139
- Friedemann C., 1969b, *Astron. Nachr.* 291, 177
- Friedemann C., Gürtler J., Schmidt R., Dorschner J., 1981, *Ap&SS* 79, 405
- Gail H.-P., Sedlmayr E., 1988, *A&A* 206, 153
- Gallino R., Busso M., Picchio G., Raiteri C.M., 1990, *Nat* 348, 298
- Gallino R., Raiteri C.M., Busso M., Matteucci F., 1994, *ApJ* 430, 858
- Gauger A., Gail H.-P., Sedlmayr E., 1990, *A&A* 235, 345
- Gilman R.C., 1969, *ApJ* 155, L185
- Goebel J.H., Chessemann P., Gerbaut F., 1995, *ApJ* 449, 246
- Gürtler J., Kömpe C., Henning Th., 1996, *A&A* 305, 878
- Hackwell J.A., 1972, *A&A* 21, 239
- Hill H., D’Hendecourt L., Perron C., Jones A., 1997, *Meteorit. Planet. Sci.* 32, 713
- Höfner S., Dorfi E.A., 1997, *A&A* 319, 648
- Höfner S., Feuchtinger M., Dorfi E.A., 1995, *A&A* 297, 815
- Höfner S., Jørgensen U.G., Loidl R., Aringer B., 1998, *A&A* 340, 497
- Hoppe P., Amari S., Zinner E., et al., 1994, *ApJ* 430, 870
- Hoppe P., Ott U., 1997, *Mainstream Silicon Carbide Grains from Meteorites*. In: Bernatowicz T., Zinner E. (eds.) *Astrophysical Implications of the Laboratory Study of Presolar Materials*. AIP 402, New York, p. 27
- Huffman D.R., 1988, *Methods and Difficulties in Laboratory Studies of Cosmic Dust Analogues*. In: Bussoletti E., Fusco C., Longo G. (eds.) *Experiments on Cosmic Dust Analogues*. Kluwer Academic Publishers, p. 25
- Huss G.R., Lewis R.S., 1994, *Meteoritics* 29, 791
- Jäger C., Mutschke H., Henning Th., 1998, *A&A* 332, 291
- Jørgensen U.G., 1988, *Nat* 332, 702
- Koike C., Hasegawa H., Manabe A., 1980, *Ap&SS* 67, 495
- Krüger C., Patzer A.B.C., Sedlmayr E., 1996, *A&A* 313, 891
- Lewis R.S., Tang M., Wacker J.F., et al., 1987, *Nat* 326, 160
- Lewis R.S., Anders E., Draine B.T., 1989, *Nat* 339, 117
- Maron N., 1990, *Ap&SS* 172, 21
- Martin P.G., Rogers C., 1987, *ApJ* 322, 374
- Mutschke H., Dorschner J., Henning Th., et al., 1995, *ApJ* 454, L157
- Mutschke H., Andersen A.C., Clément D., et al., 1999, *A&A*, 345, 187
- Ott U., 1993, *Nat* 364, 25
- Papoular R., Cauchetier M., Begin S., LeCaer G., 1998, *A&A* 329, 1035
- Preibisch Th., Ossenkopf V., Yorke H.W., Henning Th., 1993, *A&A* 279, 577
- Rouleau F., Martin P.G., 1991, *ApJ* 377, 526
- Sedlmayr E., 1994, *From Molecules to Grains*. In: Jørgensen U.G. (ed.) *Molecules in the Stellar Environment*. LNP 428, Springer-Verlag, p. 163
- Sopka R.J., Hildebrand R.H., Jaffe D.T., et al., 1985, *ApJ* 294, 242
- Speck A.K., Hofmeister A.M., Barlow M.J., 1999, *ApJ* 513, L87
- Spitzer W.G., Kleinman D.A., Frosch C.J., 1959a, *Phys. Rev.* 113(1), 133
- Spitzer W.G., Kleinman D.A., Walsh D., 1959b, *Phys. Rev.* 113(1), 127
- Stephens J.R., 1980, *ApJ* 237, 450
- Treffers R., Cohen M., 1974, *ApJ* 188, 545
- Windsteig W., Dorfi E.A., Höfner S., et al., 1997, *A&A* 324, 617
- Winters J.M., Fleischer A.J., Gauger A., Sedlmayr E., 1994, *A&A* 290, 623
- Zubko V.G., Menella V., Colangeli L., Bussoletti E., 1996, *MNRAS* 282, 1321